

Anti-interference ability of spiking neuron-astrocyte networks in working memory

Lin Li(李琳), Bingyi Mo(莫冰毅), Shanshan Cheng(程姗姗), Zhouchao Wei(魏周超), Ming Yi(易鸣), and Lulu Lu(鹿露露)

Citation: Chin. Phys. B, 2026, 35 (**6**): 068703. DOI: 10.1088/1674-1056/ae4e8c
http://cpb.iphy.ac.cn; http://iopscience.iop.org/cpb

What follows is a list of articles you may be interested in

Influences of short-term and long-term plasticity of memristive synapse on firing activity of neuronal network

Zhi-Jun Li(李志军) and Jing Zhang(张晶)
Chin. Phys. B, 2024, 33 (**12**): 128701. DOI: 10.1088/1674-1056/ad84c5

A solution method for decomposing vector fields in Hamilton energy

Xin Zhao(赵昕), Ming Yi(易鸣), Zhou-Chao Wei(魏周超), Yuan Zhu(朱媛), and Lu-Lu Lu(鹿露露)
Chin. Phys. B, 2024, 33 (**9**): 098702. DOI: 10.1088/1674-1056/ad5a74

Effect of short-term plasticity on working memory

Fan Yang(杨帆) and Feng Liu(刘锋)
Chin. Phys. B, 2023, 32 (**11**): 118706. DOI: 10.1088/1674-1056/acf03a

Computational model investigating the effect of magnetic field on neural-astrocyte microcircuit

Li-Cong Li(李利聪), Jin Zhou(周瑾), Hong-Ji Sun(孙洪吉), Peng Xiong(熊鹏), Hong-Rui Wang(王洪瑞), Xiu-Ling Liu(刘秀玲), and Chang-Yong Wang(王常勇)
Chin. Phys. B, 2021, 30 (**6**): 068702. DOI: 10.1088/1674-1056/abea81

Astrocyte and ions metabolism during epileptogenesis: A review for modeling studies

Meng-Meng Du(独盟盟), Jia-Jia Li(李佳佳), Zhi-Xuan Yuan(袁治轩), Yong-Chen Fan(范永晨), Ying Wu(吴莹)
Chin. Phys. B, 2020, 29 (**3**): 038701. DOI: 10.1088/1674-1056/ab6961

SPECIAL TOPIC — Biophysical circuits: Modeling & applications in neuroscience

Anti-interference ability of spiking neuron-astrocyte networks in working memory

Lin Li(李琳)[1], Bingyi Mo(莫冰毅)[1], Shanshan Cheng(程姗姗)[1], Zhouchao Wei(魏周超)[2], Ming Yi(易鸣)[1], and Lulu Lu(鹿露露)[1,†]

[1] *School of Mathematics and Physics, China University of Geosciences, Wuhan* 430074, *China*
[2] *Institute for Advanced Marine Research, China University of Geosciences, Guangzhou* 511462, *China*

(Received 16 January 2026; revised manuscript received 5 March 2026; accepted manuscript online 7 March 2026)

Working memory is a fundamental aspect of brain cognitive function. Its anti-interference ability relies on the network structure and the balance between excitatory and inhibitory neurons in neural systems. Here, we discuss the resistance of the spiking neuron-astrocyte network (SNAN) to noise interference of the input signal during working memory tasks, and we underscore that astrocytes play an essential regulatory role in synaptic plasticity. These results indicate that, compared to the SNAN and spiking neuron network (SNN), the improved SNAN incorporated 2-Arachidonoylglycerol (2-AG) modulation displays notable resistance to high noise interference. The improved SNAN shows optimal working memory performance, demonstrating a greater correlation between recalled patterns and input patterns. This may be due to the reduced connection sparsity of the neural network and decreased neural firing frequency caused by 2-AG, as well as its simultaneous impact on the secretion of glutamate. At the same time, astrocytes affecting memory maintenance generate overlapping calcium signals in multi-task working memory. In addition, astrocytes can significantly enhance working memory performance by modulating synaptic coupling under high noise interference. This study may provide insights into understanding the role of astrocytes in the neural mechanisms of working memory and information processing.

Keywords: working memory, astrocytes, anti-interference ability, spiking neuron-astrocyte network, synaptic plasticity

PACS: 87.19.L–, 05.45.–a, 87.19.ll, 87.19.lw

DOI: 10.1088/1674-1056/ae4e8c **CSTR:** 32038.14.CPB.ae4e8c

1. Introduction

Within the hierarchical structure of the memory system, working memory (WM) serves as a critical hub linking transient sensory information to long-term memory.[1] It undertakes the functions of short-term information storage, real-time processing, and dynamic updating, and is a prerequisite for accomplishing complex cognitive tasks such as problem-solving and decision-making.[2,3] From a neurophysiological perspective, information processing in working memory does not rely on a single brain region. Instead, it is achieved through a distributed neural circuit centered on the prefrontal cortex (PFC), which collaborates with the parietal cortex, temporal cortex, and hippocampus.[4–6] Pyramidal neurons in the prefrontal cortex maintain information storage through sustained excitatory firing, while inhibitory interneurons regulate their firing frequency and synchrony, ensuring the balance of neural circuits and the specificity of information coding.[7,8]

With the advancement of neuroscience technologies, the traditional understanding that neurons dominate neural circuits has been challenged. As the most abundant glial cells in the central nervous system, astrocytes do not merely fulfill passive functions such as structural support and nutrient supply. Instead, they form a tripartite synapse network with neurons and synapses, and deeply participate in the regulation of working memory through bidirectional signaling.[9,10] In the information processing of the tripartite synapse, glutamate released by presynaptic neurons not only acts on postsynaptic neurons to induce membrane potential changes but also activates mGluR receptors on the surface of astrocytes, triggering an increase in intracellular calcium ion concentration.[11] Endocannabinoids (e.g., 2-arachidonoylglycerol, 2-AG) released by postsynaptic neurons regulate astrocytic calcium signaling pathways and the release of gliotransmitters by binding to CB1 receptors on astrocytes.[12,13] These gliotransmitters further modulate synaptic neurotransmitter release probability and NMDA receptor-mediated synaptic plasticity, enabling precise regulation of the encoding, maintenance, and retrieval of working memory.[14] In addition, astrocytes possess multiband signal transmission capabilities; millisecond-to-second calcium signals respond to transient information, while second-to-minute metabolic signals participate in long-term processing. This characteristic allows them to efficiently cooperate with neurons, encode diverse working memory information, and determine the upper limit of storage capacity.[15–17]

[†]Corresponding author. E-mail: lululu@cug.edu.cn

© 2026 Chinese Physical Society and IOP Publishing Ltd. All rights, including for text and data mining, AI training, and similar technologies, are reserved.

The cognitive environment of the biological brain is not ideally interference-free. External visual and auditory noise, as well as internal perturbations, such as random fluctuations in neural activity and inherent variability in synaptic transmission, can threaten the stable storage and processing of working memory information.[18] Nevertheless, the human brain can still maintain efficient and stable working memory performance. Its innate anti-interference capacity provides significant biological inspiration for the construction of robust brain-inspired intelligence models.[19,54,55] Traditional spiking neural network (SNN) models primarily regulate synaptic connection strength by incorporating synaptic plasticity mechanisms, and exhibit certain anti-interference capabilities under simple interference scenarios such as Gaussian white noise and salt-and-pepper noise.[20,21] Some studies adjust the update rules of synaptic weights dynamically to enable models to encode information under noise interference, but there exists a trade-off between improved robustness and decreased accuracy — enhanced network fault tolerance reduces the recognition precision of target information. The random heterogeneous spiking neural network (RandHet-SNN) improves network adaptability to noise and reduces performance fluctuations under different noise intensities by randomizing key neuron parameters such as time constants and membrane potential thresholds.[22,23] Despite certain breakthroughs in anti-interference performance, these improved models all rely on engineering optimization strategies. This results in insufficient biological interpretability for the enhanced robustness, making it difficult to essentially replicate the anti-interference advantages of the biological brain. The emergence of the spiking neuron-astrocyte network (SNAN) model provides a new approach to addressing this issue of biological interpretability. Original SNAN models successfully recapitulated the encoding and maintenance of working memory by simplifying astrocytic calcium signaling models to simulate bidirectional neuron-astrocyte interactions.[31,47] In delayed matching task simulations, the model achieved short-term storage of target stimulus information through their cooperation, with performance highly consistent with neural activity patterns observed in biological experiments.[24,25] Existing SNAN models have significant limitations. First, they fail to integrate regulatory pathways of key endocannabinoids such as 2-Arachidonoylglycerol (2-AG) — a core pathway for tripartite synapses to maintain neural circuit balance, where 2-AG regulates astrocytic functions via CB1 receptors — rendering the models unable to truly recapitulate the anti-interference logic of biological neural circuits.[26] Second, most related studies focus on their working memory performance in noise-free or low-noise environments, without systematically investigating performance changes under different noise intensities, thus failing to clarify the astrocytes' regulatory role in maintaining working memory stability in noisy environments.[27,28]

To address the aforementioned research gaps, this study proposes an improved SNAN model integrated with the endocannabinoid (2-AG) regulatory mechanism. It aims to resolve issues such as insufficient biological interpretability and incomplete simulation of anti-interference mechanisms in existing models by accurately mimicking the molecular and cellular regulatory processes of the biological tripartite synapse network. The core innovations of the improved model lie in two aspects: (1) Integration of the 2-AG biosynthetic process, CB1 receptor-mediated signal transduction pathway, and glial transmitter release/regulation mechanisms into the SNAN framework. Astrocytes dynamically modulate the synaptic coupling strength of networks and enhance network heterogeneity to mimic the diverse intercellular interactions in biological tripartite synapses. This enables high-fidelity recapitulation of the structure and function of biological neural circuits.[29–31] (2) Design of working memory simulations with multi-level noise intensity gradients, systematically comparing the working memory accuracy (C_{P}) of the improved SNAN model, traditional SNAN model (without 2-AG regulation), and SNN model; quantitatively clarifying the gain effects of astrocytes and 2-AG pathway activation on the model's anti-interference performance, providing computational validation for the anti-interference mechanism of networks.

In this paper, 2-AG and glial transmitter modulation are introduced to the neuron–astrocyte network (SNAN) to better mimic the brain's network. The network topology is constructed using Izhikevich neurons and astrocyte networks, constituting the first key attribute. Astrocytes modulate by integrating neuronal information, adjusting their dynamics, and providing feedback to neurons. Spike-timing-dependent plasticity (STDP) is utilized to adjust the synaptic weight of the improved SNAN for increased heterogeneity, the second key attribute. The resulting astrocyte network model, integrating these attributes, is named the improved SNAN model.

2. Model and method

2.1. Spiking neuron-astrocyte network

The design of the network framework is crucial for constructing neuron–astrocyte network models and for understanding the mechanisms underlying the formation and maintenance of working memory. In this paper, the improved SNAN model shown in Fig. 1(a) is adopted, which employs a 2D grid-structured neuronal network. Each pixel in the 79×79 input layer is connected to one neuron in the $L \times H$ (79×79) neuronal layer, and the network nodes use the Izhikevich model. Each neuron can be randomly connected to up to 40 other neurons, and the neuronal layer is connected to the

next astrocyte layer via nearest-neighbor connections. Experiments have shown that cortical astrocytes in the human brain contact an average of 4 to 8 neuronal somata.[56–58] Therefore, each astrocyte is assumed to interact with a 4×4 rectangular region of neurons, and the astrocyte network adopts a $W \times T$ (26×26) square structure. The grayscale values of the input images are converted into input currents $I^{\text{Iapp}}_{(i,j)}$ and mapped onto the 79×79 neurons to provide input signals for the network model.

The tripartite synapse involves neurons and astrocytes, and their regulatory process in working memory is shown in Figs. 1(b) and 1(c), separately. First, activated presynaptic neurons (PrSNs) release glutamate, which activates mGluRs on postsynaptic neurons (PoSNs) and astrocytes to send messages (in regulation process 2).

If PoSNs are excited strongly enough, they generate an action potential and release 2-AG, an endogenous cannabinoid that acts on astrocyte type 1 cannabinoid receptors (CB1Rs) (in regulation processes 3 and 4). Glutamate and 2-AG interact with astrocyte receptors, triggering the intracellular production of inositol 1,4,5-trisphosphate (IP_3). IP_3 binds to IP_3 receptors on the ER, releasing stored calcium into the cytoplasm (in regulation processes 5 and 6). Information is converted into neuronal spikes, and Ca^{2+} waves are produced in the astrocyte network to encode and transmit information. When the Ca^{2+} concentration in astrocytes reaches a specific threshold, they release gliotransmitters such as glutamate (in regulation process 7). These gliotransmitters interact with mGluRs on neurons, resulting in indirect excitatory effects on PrSNs, referred to as endogenous cannabinoid-mediated synaptic potentiation (e-SP). Astrocytes release gliotransmitters in response to synchronized neuronal activity when Ca^{2+} concentrations exceed 0.15 μm. Astrocyte activity impacts all connected neurons and is key for working memory. It involves over 50% of neurons activating together and is simulated by each neuron's activated input synapses.[32,33]

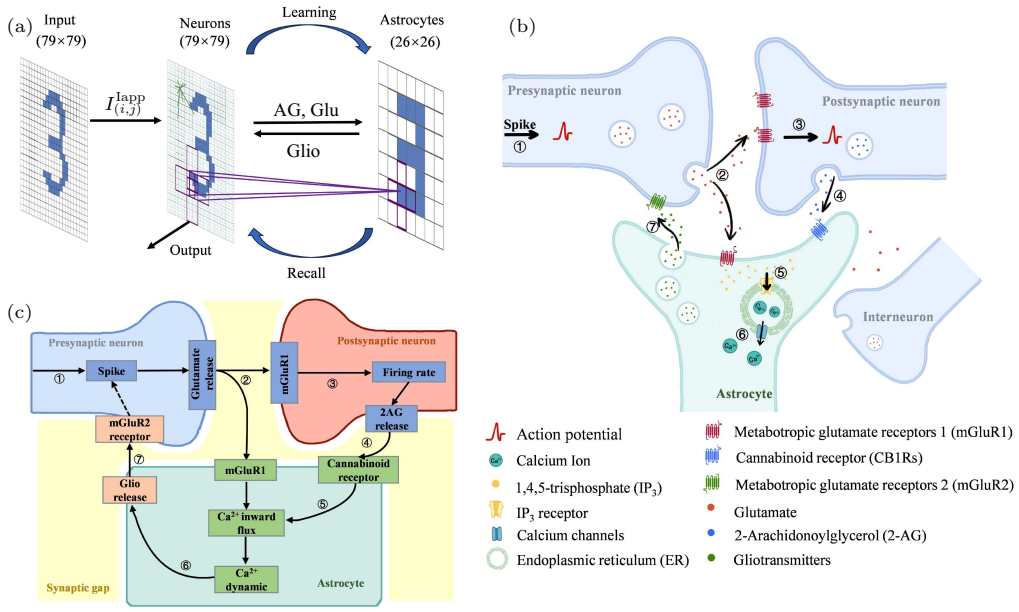


Fig. 1. Schematic representation of the neuron–astrocyte network and its tripartite synaptic regulatory mechanisms. (a) Model of neuron–astrocyte networks. Model includes a pulsatile neural network ($L \times H$) and an astrocyte network ($W \times T$), characterized by specific neuronal connections. Raw images are transformed into current signals and input into the network, with the output represented as the average firing rate of neurons, indicating memory recall. (b) Tripartite modulation of synapses. (c) Working memory regulation process.

2.1.1. Spiking neural network

The Izhikevich model describes neuronal dynamics in spiking neural networks, enabling efficient computation while preserving biological accuracy. The model[34,35] is given by

$$\begin{aligned} \frac{\mathrm{d}V_{(i,j)}}{\mathrm{d}t} &= 0.04V^2_{(i,j)} + 5V_{(i,j)} - U_{(i,j)} + 140 + I^{\text{Iapp}}_{(i,j)} + I^{\text{syn}}_{(i,j)}, \\ \frac{\mathrm{d}U_{(i,j)}}{\mathrm{d}t} &= a(bV_{(i,j)} - U_{(i,j)}), \end{aligned} \tag{1}$$

and the auxiliary after-spike reset:

$$\text{if} \quad V_{(i,j)} \geq 30\ \text{mV}, \quad \text{then} \begin{cases} V_{(i,j)} \leftarrow c, \\ U_{(i,j)} \leftarrow U_{(i,j)} + d, \end{cases} \tag{2}$$

where $V_{(i,j)}$ represents the membrane potential of neuron (i,j) ($i, j = 1, \ldots, 79$), and $U_{(i,j)}$ signifies the recovery variable of the neuron. The parameters are defined as $a = 0.1$, $b = 0.2$, $c = -65$ mV, and $d = 2$.[36,37] $I^{\text{Iapp}}_{(i,j)}$ represents the external input current signal. The synaptic current $I^{\text{syn}}_{(i,j)}$, generated by excitatory and inhibitory synapses, is calculated as[31,38,39]

$$\begin{aligned} I^{\text{syn}}_{(i,j)} &= I^{\text{synE}}_{(i,j)} + I^{\text{synI}}_{(i,j)} \\ &= P_{\text{E}} \cdot \sum_{k=1}^{N^{\text{E}}} \frac{g^{\text{syn}}_{(i,j)} (E_{\text{synE}} - V_{(i,j)})}{1 + \exp\left(\frac{-V^k_{\text{pre}}}{k_{\text{syn}}}\right)} + (1 - P_{\text{E}}) \end{aligned}$$

$$\times \sum_{k=1}^{N^{\mathrm{I}}} \frac{g^{\mathrm{syn}}_{(i,j)}\left(E_{\mathrm{synI}} - V_{(i,j)}\right)}{1+\exp\left(\frac{-V^{k}_{\mathrm{pre}}}{k_{\mathrm{syn}}}\right)}, \tag{3}$$

where $I^{\mathrm{synE}}_{(i,j)}$ and $I^{\mathrm{synI}}_{(i,j)}$ represent excitatory and inhibitory synaptic currents, and P_{E} denotes the fraction of excitatory neurons. E_{synE} and E_{synI} represent the reversal potentials of excitatory and inhibitory synapses, respectively. The term V_{pre} denotes the membrane potential of PrSNs.

Here, $g^{\mathrm{syn}}_{(i,j)}$ represents neural synaptic coupling,

$$g^{\mathrm{syn}}_{(i,j)} = w_{(i,j)} + g^{\mathrm{Astro}}_{(i,j)}, \tag{4}$$

where the synaptic weight $w_{(i,j)}$ is dynamically modified for the synaptic coupling only during the training phase using the spike-timing dependent plasticity (STDP) rule. The synaptic weights are initialized at 0.0001, and the maximum weight is denoted as $w_{\max}$. The precise update rule is[40–42]

$$w_{(i,j),k}(t+1) = \begin{cases} w_{(i,j),k}(t) + \eta \exp(\Delta t/\tau), & \Delta t \geq 0, \\ w_{(i,j),k}(t) - \eta \exp(\Delta t/\tau), & \Delta t \leq 0, \end{cases}$$

$$w_{(i,j),k} \in [0.0001, w_{\max}], \tag{5}$$

where τ (= 20 ms) represents the time constant of the PrSN and PoSN traces, η denotes the greatest change in synaptic weights, and Δt signifies the time interval between the firing of the presynaptic neuron and the postsynaptic neuron.

The ratio of activated synapses to total connections is

$$SoI^{\mathrm{syn}}_{(i,j)} = \frac{N^{\mathrm{Activated}}_{\mathrm{out}}}{N_{\mathrm{out}}}, \tag{6}$$

where N_{out} ($= N^{\mathrm{E}} + N^{\mathrm{I}}$) represents the total connective number for each neuron linked to the other 40 neurons, and the number of activated neurons is $N^{\mathrm{Activated}}_{\mathrm{out}}$.

2.1.2. Astrocyte network

The astrocyte network dynamics involve calcium ions (Ca^{2+}), inositol 1,4,5-trisphosphate (IP_3), and the proportion of activated IP_3 receptors (h). The dynamics are calculated using the Ullah model:[43]

$$\begin{cases} \dfrac{\mathrm{d}[\mathrm{Ca}^{2+}]_{(m,n)}}{\mathrm{d}t} = J^{\mathrm{ER}}_{(m,n)} + J^{\mathrm{in}}_{(m,n)} - J^{\mathrm{out}}_{(m,n)} + J^{\mathrm{leak}}_{(m,n)} - J^{\mathrm{pump}}_{(m,n)} + \mathrm{diff}^{\mathrm{Ca}}_{(m,n)} - \zeta W_{(m,n)}, \\ \dfrac{\mathrm{d}[\mathrm{IP}_3]_{(m,n)}}{\mathrm{d}t} = \dfrac{[\mathrm{IP}^{*}_3] - [\mathrm{IP}_3]_{(m,n)}}{\tau_{\mathrm{IP3}}} + J^{\mathrm{Glu}}_{(m,n)} + J^{\mathrm{AG}}_{(m,n)} + J^{\mathrm{PLC}\delta}_{(m,n)} + \mathrm{diff}^{\mathrm{IP_3}}_{(m,n)}, \\ \dfrac{\mathrm{d}h_{(m,n)}}{\mathrm{d}t} = a_2\left(d_2\dfrac{[\mathrm{IP}_3]_{(m,n)}+d_1}{[\mathrm{IP}_3]_{(m,n)}+d_3}(1-h_{(m,n)}) - h_{(m,n)}[\mathrm{Ca}^{2+}]_{(m,n)}\right), \end{cases} \tag{7}$$

where (m, n) represents the position coordinates of astrocytes (where $m, n = 1, \ldots, 26$). $[\mathrm{Ca}^{2+}]_{(m,n)}$ represents the calcium concentration in the cytoplasm of astrocytes, $[\mathrm{IP}_3]_{(m,n)}$ indicates the steady-state concentration of IP_3, and h is the fraction of the endoplasmic reticulum (ER) surface covered by activated IP_3 receptors. $W_{(m,n)}$ refers to the activity window as defined in Eq. (19), and ζ indicates the efficacy factor of calcium ions in relation to active cellular depletion. The fluxes are defined:

$$\begin{cases} J^{\mathrm{ER}} = c_1 v_1 [\mathrm{Ca}^{2+}]^3 h^3 [\mathrm{IP}_3]^3 \dfrac{\left(c_0/c_1 - (1+1/c_1)[\mathrm{Ca}^{2+}]\right)}{\left(([\mathrm{IP}_3]+d_1)\left([\mathrm{Ca}^{2+}]+d_4\right)\right)^3}, \\ J^{\mathrm{in}} = \dfrac{v_5[\mathrm{IP}_3]^2}{k_2^2+[\mathrm{IP}_3]^2}, \\ J^{\mathrm{out}} = k_1[\mathrm{Ca}^{2+}], \\ J^{\mathrm{leak}} = c_1 v_2\left(c_0/c_1 - (1+1/c_1)[\mathrm{Ca}^{2+}]\right), \\ J^{\mathrm{pump}} = \dfrac{v_3[\mathrm{Ca}^{2+}]^2}{k_3^2+[\mathrm{Ca}^{2+}]^2}, \\ J^{\mathrm{PLC}\delta} = \dfrac{v_4\left([\mathrm{Ca}^{2+}]+(1-\alpha)k_4\right)}{[\mathrm{Ca}^{2+}]+k_4}, \end{cases} \tag{8}$$

where J^{ER} represents the calcium flux from the endoplasmic reticulum to the cytoplasm. J^{in} and J^{out} indicate the exchange of calcium ions with the extracellular space. J^{leak} refers to the leakage flux from the endoplasmic reticulum to the cytoplasm, J^{pump} denotes the flux of calcium pumped from the cytoplasm back to the endoplasmic reticulum, and $J^{\mathrm{PLC}\delta}$ signifies the flux of IP_3 produced by phospholipase C.

Cortical astrocytes are interconnected via Cx43 gap junctions, and calcium ions and IP_3 molecules traverse these junctions. $\mathrm{diff}^{\mathrm{IP_3}}_{(m,n)}$ and $\mathrm{diff}^{\mathrm{Ca}}_{(m,n)}$ denote the diffusion of calcium ions through the gap junctions:[44]

$$\begin{cases} \mathrm{diff}^{\mathrm{IP_3}}_{(m,n)} = d_{\mathrm{IP_3}}(\Delta[\mathrm{IP}_3])_{(m,n)}, \\ \mathrm{diff}^{\mathrm{Ca}}_{(m,n)} = d_{\mathrm{Ca}}(\Delta[\mathrm{Ca}^{2+}])_{(m,n)}, \end{cases} \tag{9}$$

where $d_{\mathrm{IP_3}}$ and d_{Ca} represent the diffusion rates of IP_3 and calcium, respectively. Each astrocyte is diffusely coupled to its four nearest neighbors as defined by the Laplace operator Δ:

$$\begin{cases} (\Delta[\mathrm{IP}_3])_{(m,n)} = (\Delta[\mathrm{IP}_3])_{(m-1,n)} + (\Delta[\mathrm{IP}_3])_{(m+1,n)} \\ \qquad\qquad + (\Delta[\mathrm{IP}_3])_{(m,n-1)} + (\Delta[\mathrm{IP}_3])_{(m,n+1)} \\ \qquad\qquad - 4(\Delta[\mathrm{IP}_3])_{(m,n)}, \\ (\Delta[\mathrm{Ca}^{2+}])_{(m,n)} = (\Delta[\mathrm{Ca}^{2+}])_{(m-1,n)} + (\Delta[\mathrm{Ca}^{2+}])_{(m+1,n)} \\ \qquad\qquad + (\Delta[\mathrm{Ca}^{2+}])_{(m,n-1)} + (\Delta[\mathrm{Ca}^{2+}])_{(m,n+1)} \\ \qquad\qquad - 4(\Delta[\mathrm{Ca}^{2+}])_{(m,n)}. \end{cases} \tag{10}$$

2.1.3. Bidirectional neuron-astrocyte interaction

Glutamate interacts with metabotropic glutamate receptors 1 (mGluR1) located on the membranes of postsynaptic neurons and astrocytes. The dynamics of glutamate concentration are

$$\frac{\mathrm{d}\mathrm{Glu}_{(i,j)}}{\mathrm{d}t} = -\frac{\mathrm{Glu}_{(i,j)}}{\tau_{\mathrm{Glu}}} + r_{\mathrm{Glu}} \times SoI^{\mathrm{syn}}_{(i,j)}, \tag{11}$$

where $\mathrm{Glu}_{(i,j)}$ represents the concentration of glutamate release, r_{Glu} indicates the release rate, and τ_{Glu} is the decay rate. The 2-AG is released by postsynaptic neurons, and its concentration $AG_{(i,j)}$ is[39,47]

$$\frac{\mathrm{d}AG_{(i,j)}}{\mathrm{d}t} = -\alpha_{\mathrm{AG}} AG_{(i,j)} + k_{\mathrm{AG}} \Theta(V_{(i,j)} - 30), \tag{12}$$

where α_{AG} ($= 10\ \mathrm{s}^{-1}$) represents the clearance constant of 2-AG, k_{AG} ($= 600\ \mu\mathrm{M}{\cdot}\mathrm{s}^{-1}$) denotes the release efficacy of 2-AG, and Θ signifies the Heaviside step function.

The total effector $G_{(i,j)}$ of glutamate and 2-AG collectively influences the signal response of astrocytes:

$$\mathrm{Glu}_{(i,j)} \times \gamma_{\mathrm{Glu}} + AG_{(i,j)} \times \gamma_{\mathrm{AG}} = G_{(i,j)}, \tag{13}$$

where the terms γ_{Glu} ($= 0.4$) and γ_{AG} ($= 0.6$) represent the regulatory weights of glutamate and 2-AG on astrocytes, respectively.

Astrocytes detect intense neuronal activity by the following two necessary conditions: the concentration of glutamate and 2-AG is above a certain threshold, and more than half of the neurons regulated by astrocytes reach the spiking state.

$$\frac{1}{N} \sum_{(i,j)\in N} [G_{(i,j)} > G_{\mathrm{thr}}] > F_{\mathrm{act}}, \tag{14}$$

where G_{thr} ($= 0.7\ \mu\mathrm{M}$) represents the threshold concentration of the neurotransmitter that elicits the astrocyte response, and $[\cdot]$ denotes the Iverson bracket. The term F_{act} ($= 0.5$) represents the proportion of spiking neurons. J^{Glu} and J^{AG} collectively stimulate the generation of IP_3:

$$J^{\mathrm{Glu}} + J^{\mathrm{AG}} = \begin{cases} A_{\mathrm{G}}, & \text{if } t_0 < t \le t_0 + t_{\mathrm{G}}, \\ 0, & \text{otherwise}, \end{cases} \tag{15}$$

where the rectangular pulse exhibits amplitude A_{G} ($5\ \mu\mathrm{M}{\cdot}\mathrm{s}^{-1}$) and duration t_{G} (60 ms). The term t_0 indicates the moment when the neurotransmitter concentration $G_{(i,j)}$ fulfills Eq. (14).

Table 1. Parameters of the improved spiking neuron–astrocyte network model.[24]

Parameter	Parameter description	Value
E_{synE}	Synaptic reversal potential of excitatory synapses	0 mV
E_{synI}	Synaptic reversal potential of inhibitory synapses	−90 mV
k_{syn}	The slope of the synaptic activation function	0.2 mV
c_0	Cytosolic volume of total Ca^{2+}	2.0 μM
c_1	ER-cytosol Ca^{2+} dynamics determiner	0.185
v_1	Max Ca^{2+} channel flow rate	$6\ \mathrm{s}^{-1}$
v_2	Ca^{2+} leakage rate control	$0.11\ \mathrm{s}^{-1}$
v_3	Max Ca^{2+} uptake capacity	$2.2\ \mu\mathrm{M}{\cdot}\mathrm{s}^{-1}$
v_4	Maximum rate for IP_3 production	$0.3\ \mu\mathrm{M}{\cdot}\mathrm{s}^{-1}$
v_5	Max rate of activation Ca^{2+} influx	$0.2\ \mu\mathrm{M}{\cdot}\mathrm{s}^{-1}$
k_1	Ca^{2+} extrusion rate constant	$0.5\ \mathrm{s}^{-1}$
k_2	The half-saturation constant of agonist-dependent Ca^{2+} entry	1 μM
k_3	ATP–Ca^{2+} pump activation constant	0.1 μM
k_4	Dissociation constant of Ca^{2+}-stimulation IP_3 production	1.1 μM
a_2	Ca^{2+} inhibition constant	$0.14\ \mu\mathrm{M}^{-1}{\cdot}\mathrm{s}^{-1}$
d_1	Dissociation constant for IP_3	0.13 μM
d_2	Dissociation constant of Ca^{2+} inhibition	1.049 μM
d_3	Dissociation constant of the IP_3 receptor	0.9434 μM
d_4	Ca^{2+} activation constant	0.08234 μM
α	Ca^{2+} reaction rate constant	0.8
$1/\tau_{\mathrm{IP3}}$	Loss rate of IP_3	$0.14\ \mathrm{s}^{-1}$
$[\mathrm{IP}_3^*]$	Steady-state IP_3 level	0.16 μM
d_{IP3}	IP_3 diffusion speed	$0.1\ \mathrm{s}^{-1}$
d_{Ca}	Ca^{2+}diffusion speed	$0.05\ \mathrm{s}^{-1}$
r_{Glu}	Glutamate release rate	$400\ \mu\mathrm{M}{\cdot}\mathrm{s}^{-1}$
α_{AG}	the clearance constant of 2-AG	$10\ \mathrm{s}^{-1}$
k_{AG}	the release efficacy of 2-AG	$600\ \mu\mathrm{M}{\cdot}\mathrm{s}^{-1}$
γ_{Glu}	the regulatory weights of glutamate	0.4
γ_{AG}	the regulatory weights of 2-AG	0.6
t_{WM}	the WM duration	250 ms
$[Ca^{2+}]_{\mathrm{Thr}}$	required Ca^{2+}concentration to WM activity	0.15 μM
G_{thr}	the threshold concentration of neurotransmitter	0.7 μM

2.2. Working memory performance mechanisms

Astrocyte activity facilitates WM by enhancing the efficacy of all synapses within their vicinity.[52,53] This activity is initiated upon the fulfillment of two specific conditions:[26,45]

$$\begin{cases} [\mathrm{Ca}^{2+}]_{(m,n)}] \geq [\mathrm{Ca}^{2+}]_{\mathrm{Thr}}, \\ F_{\mathrm{spike}} \geq F_{\mathrm{Recall}} \times N_{\mathrm{a}}, \end{cases} \tag{16}$$

where N_{a} ($=16$) indicates the number of neurons connected to astrocytes. Equation (16) must be met. F_{Recall} must be at least 0.50, meaning that at least 8 out of 16 neurons must fire synchronously; the calcium ion concentration in astrocytes must exceed the threshold $[\mathrm{Ca}^{2+}]_{\mathrm{Thr}}$ of 0.15 μm. The activity window $W_{(m,n)}$ regulates the release of gliotransmitters with a duration of t_{WM}:

$$W_{(m,n)} = \begin{cases} 1, & t_0 < t \leq t_0 + t_{\mathrm{WM}}, \\ 0, & \text{otherwise}, \end{cases} \tag{17}$$

where t_0 is the start time that satisfies Eq. (16). The working memory window duration t_{WM} ($=250$ ms), includes the input sample duration (0.15 s) and the input interval time (0.1 s).

$\mathrm{Gli}_{(m,n)}$ indicates the concentration of gliotransmitters released by active astrocytes:

$$\frac{\mathrm{dGli}_{(m,n)}}{\mathrm{d}t} = -\frac{\mathrm{Gli}_{(m,n)}}{\tau_{\mathrm{Gli}}} + r_{\mathrm{Gli}} \times W_{(m,n)}, \tag{18}$$

where τ_{Gli} ($=0.1$) and r_{Gli} ($=0.35$) denote the gliotransmitter clearance time constant and release rate, respectively. Gliotransmitter release influences how astrocytes interact with neurons. This process involves the modulation of synaptic connections, known as g^{Astro}:

$$g^{\mathrm{Astro}}_{(i,j)} = \eta \times \mathrm{Gli}_{(m,n)}, \tag{19}$$

where the term η ($=0.4$) denotes the magnitude of the modulating synaptic action.

2.3. Input stimulation

To simulate input signal distortion, salt-and-pepper noise is introduced directly into the input image to represent network noise. The salt-and-pepper noise can be expressed as the original image $f(x,y)$ corrupted by a noise process. Let the range of pixel values be [0, 255] (since the grayscale values of the input digital image range from 0 to 255), and let the noisy image be denoted as $g(x,y)$:

$$g(x,y) = \begin{cases} 0 \text{ with probability (pepper noise,black dots) } \frac{d}{2}, \\ 255 \text{ with probability } \frac{d}{2} \text{ (salt noise,white dots)}, \\ f(x,y) \text{ with probability } 1-d \text{ (uncorrupted)}, \end{cases} \tag{20}$$

where the noise intensity parameter $d \in [0,1]$ represents the probability that a pixel is corrupted by noise.

The input signals of the model adopt grayscale images of Arabic numerals. Specifically, four predefined grayscale images of numbers are used as input samples in the training phase, while eight grayscale images of numbers are randomly input in the testing phase. Among these test samples, four are matching samples (the same numbers as those in the training phase) and four are non-matching samples (four other distinct numbers not used in training). All input images are set to a resolution of 79×79 pixels, which exactly matches the scale of the spiking neural network, ensuring that the input signals can be directly mapped to the corresponding neurons. The input images have 256 grayscale levels, and these grayscale values are linearly mapped to the interval $[-10, 10]$ to serve as the input current injected into the neurons. The input current is in the form of a rectangular wave with an amplitude of 10 μA. To simulate the robustness of working memory under noise interference, the system input noise intensity is set to 0.05 in the training phase. In the testing phase, random noise with different intensities is added to the input current (with noise intensity as a variable) to verify the anti-interference ability of the model. The training phase starts at 0.5 s. Each training sample is presented for 0.2 s, with an interval of 0.1 s between consecutive samples. In the testing phase, each sample is presented for 0.15 s, with an interval of 0.25 s between samples. If a sample is correctly recognized through WM, the neurons will continue to fire for an additional 0.1 s under the modulation of astrocytes. In addition, all differential equations in the model are numerically solved using the fourth-order Runge–Kutta method, with an integration step size of 0.0001 s.

2.4. Working memory correlation and network metrics

The improved SNAN model's WM performance is measured by correlation C_{P}. The value of C_{P} varies from 0 to 1, where a higher value signifies better WM performance between recall patterns and input patterns. When the working memory performance metric is higher than 0.9, the cued recall correlation of the sample is good. The C_{P} is calculated as

$$\begin{cases} C_{\mathrm{P}} = \dfrac{1}{|T_{\mathrm{P}}|} \displaystyle\max_{t \in [t-T_{\mathrm{P}},t]} C(t), \\ C(t) = \dfrac{1}{2}\left(\dfrac{1}{|P|} \displaystyle\sum_{(i,j)\in P} M_{ij}(t) + \dfrac{1}{L \cdot H - |P|} \displaystyle\sum_{(i,j)\notin P} (1 - M_{ij}(t)) \right), \\ M_{ij}(t) = \left[\left(\displaystyle\sum_{k \in [t-f,t]} [V_{ij}(k) > TH] \right) > 0 \right], \end{cases} \tag{21}$$

where $C(t)$ denotes the correlation value in the time interval $[t - T_{\mathrm{P}}, t]$ (with $T_{\mathrm{P}} = 30$ ms). P is the set of non-zero pixels of the ideal sample, and $|P|$ is the count of these pixels. $M_{ij}(t)$ is the indicator function, yielding a value of 1 when the average discharge rate $V_{ij}(k)$ of neuron (i,j) within the interval $[t-f,t]$ (with $f = 1$ ms) surpasses the threshold TH ($=30$ mV), and 0 otherwise. $[\cdot]$ denotes the Iverson bracket.

The degree of clustering of neurons connected to other neurons is measured by the average clustering coefficient (ACC):

$$\mathrm{ACC} = \frac{1}{N}\sum_{i=1}^{N}\frac{2e_i}{D_{n_i}(D_{n_i}-1)}, \tag{22}$$

where D_{ni} represents the number of neighboring nodes of node i, e_i denotes the number of edges that exist between the neighboring nodes of node i, and N is the total number of nodes in the network. The ACC ranges from 0 to 1, where higher values signify a more pronounced clustering phenomenon in the network, that is, neighboring nodes are more likely to be directly connected to one another.[46]

3. Results and discussion

Excitatory and inhibitory balanced neurons and the synaptic connection structure are crucial for working memory in neural networks. Subsequently, the anti-interference performance and robustness mechanisms of the improved SNAN model, and the synaptic couplings on the working memory, are discussed.

3.1. Working memory under different noise intensities

In order to determine the neuron layer network structure, four complex network structures (scale-free networks, regular networks, small-world networks, and self-similar networks) were tested as shown in Fig. 2. The P_{E} value is the ratio of excitatory neurons in the spiking neural network, ranging from 0 (fully inhibitory) to 1 (fully excitatory). The shaded area represents the range of error for different samples of working memory metrics. The solid line indicates the average performance of working memory. We use mean-field theory to simplify the dynamics of the neural network by approximating the mean value of the neurons.

The C_{P} mean values of the four complex network structures all show an upward trend at low P_{E} values, followed by a tendency to stabilize, as depicted in Fig. 2(a). On average across all input images, the scale-free network performs optimally in working memory tasks across various P_{E} values. The small-world network and the regular network exhibit similar performance levels, while the self-similar network performs poorly compared to the others. The working memory performance is related to the features of the input signal, and the error bands represent the variation in memory performance for each picture. Taking the number 3 as an example, the memory recall at an excitatory neuron proportion (P_{E}) of 0.4 is depicted in Figs. 2(b)–2(d). The C_{P} for the scale-free network, the regular network, the self-similar network, and the small-world network are 0.9425, 0.8857, 0.877 and 0.9331, respectively. The scale-free network exhibits the most accurate memory performance relative to the other networks. The small-world network also shows superior performance but is noisier compared to the scale-free network. The neuron firing frequency is lower for the regular and self-similar networks. In scale-free networks, when the proportion of excitatory neurons is below 30%, the working memory performance metric C_{P} is below 0.9, and it increases as the proportion rises. When the P_{E} value is 0.4, the C_{P} value shows a small peak, eventually fluctuating between 0.93 and 0.96, providing a higher correlation. At a P_{E} value of 0.6, the average C_{P} value is 0.9460, reaching optimal performance in working memory. It is found that the proportions of excitatory and inhibitory neurons and connection structures affect working memory performance. Next, we select a scale-free network with a PE value of 0.6 to investigate its anti-interference ability in the improved SNAN model.

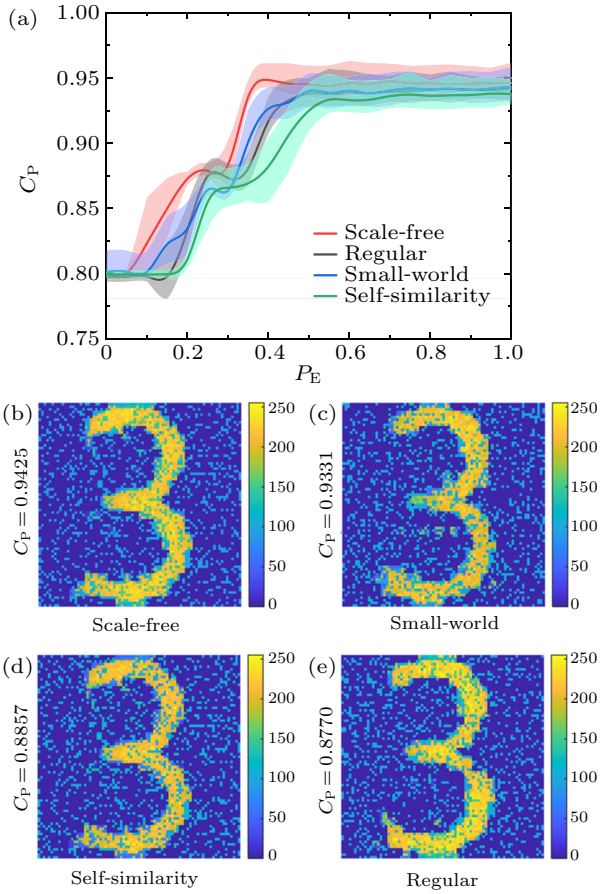


Fig. 2. Working memory metrics of four complex network structures. (a) Comparison of working memory performance under different P_{E}. Solid line represents the average working memory performance metrics for test samples 0, 1, 2 and 3, and the min–max bands denote the maximum and minimum range of working memory metrics for an individual sample. Panels (b)–(e) show the working memory recall of scale-free networks, regular networks, self-similar networks and small-world networks at $P_{\mathrm{E}} = 0.4$, respectively. The C_{P} of the four networks is labeled on the left, and the color bar on the right ranges from blue to yellow, indicating network firing rates from low to high.

During the testing stage, salt-and-pepper noise with intensities ranging from 0.02 to 0.5 is introduced into the network input to simulate signal noise interference in the working memory of the brain. Comparing the improved SNAN, SNAN, and SNN, it is found that when the noise intensity is very

low (below 0.05), there is almost no difference in the working memory performance (C_P) of the three models, all around 0.98 (Fig. 3(a)). However, under medium and high noise intensities, the spiking neuron–astrocyte network demonstrated significant interference resistance. At a medium noise intensity of 0.2, the C_P values for the improved SNAN model and the SNAN model are 0.9459 and 0.9398, respectively, allowing them to complete the working memory task almost perfectly. The C_P value for the SNN model at this point is 0.7989. At a high noise intensity level of 0.35, the average C_P values for the SNAN model and the improved SNAN model were above 0.85, while the average C_P value for the SNN model is only 0.6505, indicating that the network had almost no robustness and noise reduction capability.

The dashed gray line in Fig. 3(a), serving as a reference baseline, intersects the coordinate points (0.02, 0.98) and (0.50, 0.75). ΔC_P represents the changes in the relative differences in cognitive performance of working memory between the improved SNAN model and the SNAN model at various noise intensities. Compared to the SNAN model, the improved SNAN model has better working memory performance between noise intensities of 0.2 and 0.45, especially at noise intensities of 0.3 and 0.4 where the difference in C_P value is larger (Fig. 3(b)). This indicates that the improved SNAN model shows its advantages at medium and high noise intensities. Specifically, at a medium noise intensity of 0.20, the absolute difference in C_P values among the three models is relatively small, while the improved SNAN model demonstrates precise memory recall ability. However, the recalled images of the original SNAN model exhibit noticeable noise pixels, and the recalled images of the SNN model are almost completely covered by noise, resulting in severe loss of effective information (Fig. 3(c)). At a high noise intensity of 0.35, there is interference with the recall performance of all models to varying degrees. However, the improved SNAN model still maintains relatively clear recalled images, demonstrating its excellent working memory ability even under strong noise. Although the recalled images of the original SNAN model exhibit significant memory biases, they still retain the general outline of the original numbers. In contrast, the recalled images of the SNN model are almost cluttered with noise, completely losing their anti-interference ability (Fig. 3(c)). These results emphasize the importance of astrocytes in working memory, and reveal that refining the regulation process of 2-AG and gliotransmitters can effectively enhance the network's anti-interference capability and working memory performance.

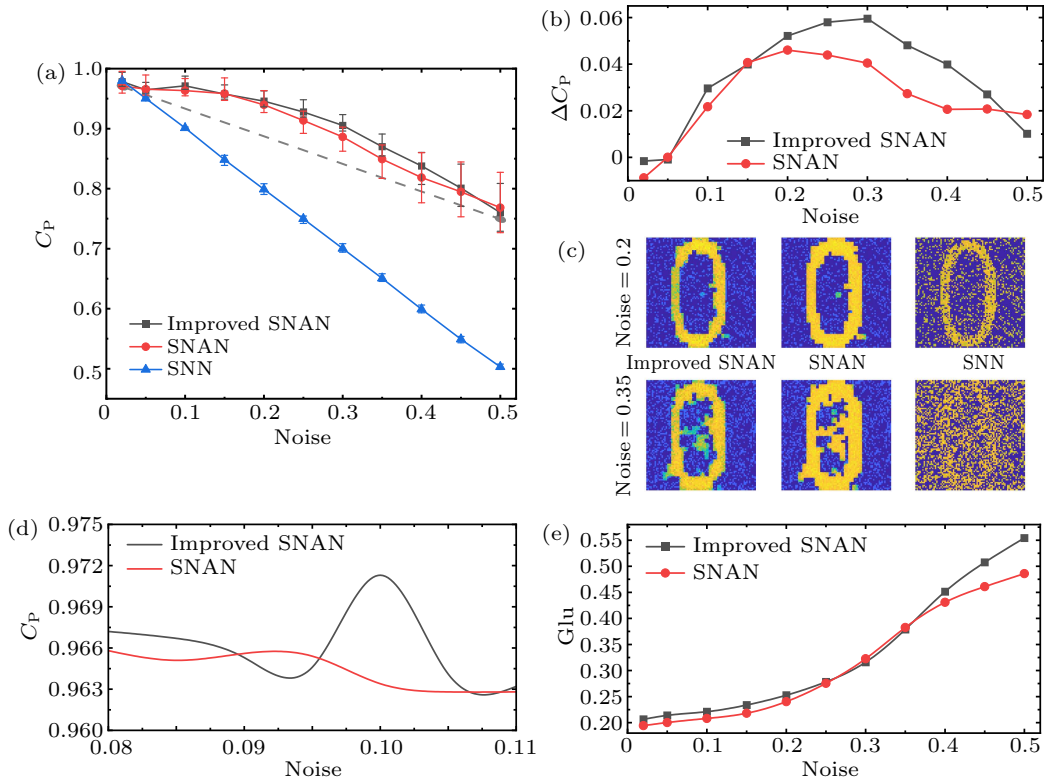


Fig. 3. (a) Comparison of working memory performance among the three models: the improved SNAN model, SNAN model, and SNN model without astrocytes. Solid line represents the mean value of working memory performance for each test image, and the min–max bars denote the maximum and minimum of working memory metrics for an individual sample. Horizontal axis represents the intensity of salt-and-pepper noise added to the input image (signal) during the testing phase. (b) Difference between the correlations of system recall and test patterns using the gray dashed line in (a) as a baseline. (c) Recall visualization for pattern 0 (neuronal firing rate). (d) Working memory performance of the model at noise intensities from 0.08 to 0.11. (e) Concentration of glutamate (Glu) in the improved SNAN and SNAN models across varying noise levels.

It is noted that within a narrow range of noise levels between 0.095 and 0.105, the performance of the improved SNAN model exhibits a significant resonance peak (Fig. 3(d)). This may be attributed to the resonance of neuronal activity with the network state, thereby enhancing the encoding and maintenance of information. In contrast, the original SNAN model does not show a similar performance peak, indicating its lower sensitivity to noise. This difference may be related to the more complex regulatory mechanisms in the improved SNAN model, such as the finer activity regulation of astrocytes, which enables an adaptive and enhanced response to noise stimuli within a specific range. Moderate noise may play a role in promoting neural network function, while excessive noise causes interference. The resonance phenomenon observed in the improved SNAN model may be an adaptive response mechanism that helps the network maintain stability in noisy environments.

From the perspective of neurochemical regulation, the improved SNAN model exhibits significantly enhanced glutamate activity under different noise intensities (Fig. 3(e)). This improvement is likely attributed to the synergistic regulation mechanism between glutamate and 2-AG, which jointly promotes the network's adaptability to noise. In contrast, the original SNAN model mainly relies on single glutamate regulation, resulting in a smaller increase in activity. These findings suggest that the improved SNAN model may regulate neuronal activity more effectively through the combined action of glutamate and 2-AG, thereby exerting a positive influence on working memory function.

Furthermore, we compare the recalled images of two specific noise intensities (0.2 and 0.35) for the working memory of the three network models. The results show that the improved SNAN model consistently achieves the highest recall performance. Due to the differences in the input image features, the model exhibits varying recall performance across the four images. At a noise intensity of 0.2, the improved SNAN network consistently demonstrates the highest recall performance, presenting the original numbers almost clearly. The recall results of the SNAN model include a small number of extra pixels. When the noise intensity increases to 0.35, the anti-interference ability of the improved SNAN model becomes the most notable, and the recalled images remain relatively clear and accurate. The SNAN model shows poor recall effects, especially for the numbers 0 and 3 (Fig. 4), where neurons fire at pixels that incorrectly memorize the image. This may be due to the SNAN network being more prone to memorizing images with more distinct or simple features. However, the SNN network is almost entirely disrupted by noise and does not demonstrate any interference resistance in the working memory task. In summary, the improved SNAN model significantly enhances the working memory robustness and anti-interference ability of the network under medium and high noise intensity by integrating a more refined astrocyte regulatory mechanism, particularly the synergistic effect of glutamate and 2-AG.

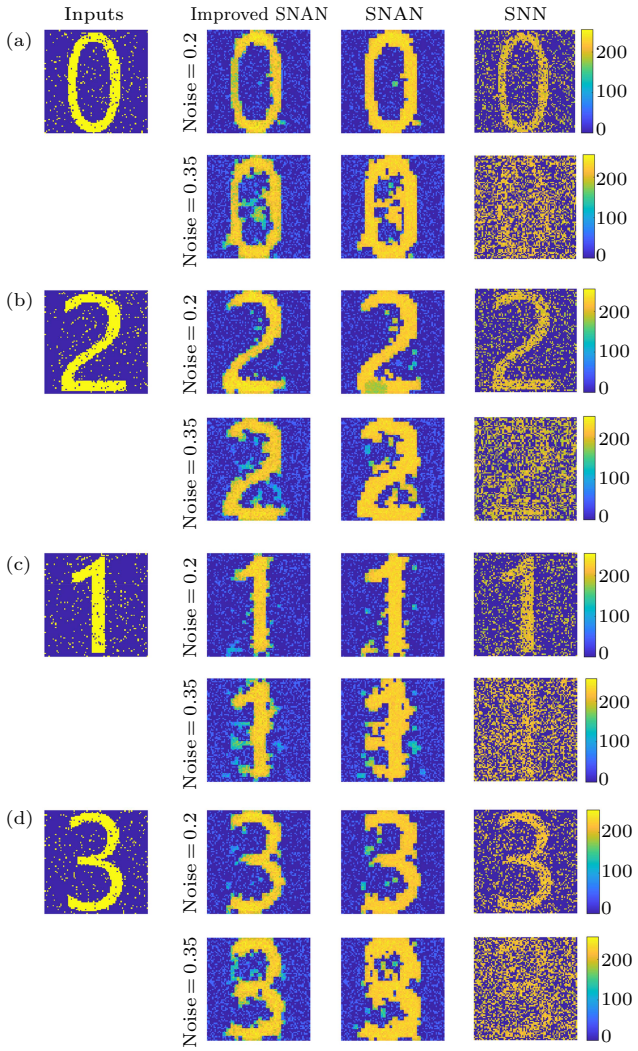


Fig. 4. Cue recall of the neuron–astrocyte network in a WM task. (a) Cue recall for the digit 0 under noise intensities of 0.2 and 0.35. Input image signal is in the first column, with columns 2–4 showing the recall for the improved SNAN, SNAN and SNN models. (b)–(d) Similar recall results for digits 2, 1, and 3.

3.2. Exploring the mechanisms of superior performance in anti-interference working memory

To achieve a deeper understanding of the mechanisms of the better anti-interference ability of the improved SNAN model, we next explore the connection aggregation and the average firing frequency of neurons, and the ACC is used to assess the local connectivity tightness of the networks. At a noise intensity of 0.2, the improved SNAN model exhibits more localized and concentrated synaptic connections. The ACC of the improved SNAN model and the SNAN model are 0.4027 and 0.4407, respectively (Figs. 5(a) and 5(c)). This difference suggests that the improved SNAN network is more

sparsely connected overall. At a high noise intensity of 0.35, both the improved SNAN model and the SNAN model exhibit a certain degree of dispersion in the network local connections (Figs. 5(b) and 5(d)). However, the improved SNAN model still has clearer localized and concentrated synaptic connections and has a lower ACC. This suggests that the modulation of 2-AG and gliotransmitters in brain working memory improves the anti-interference ability of the network and maintains working memory performance under high noise intensity.

From the perspective of working memory performance C_{P}, it declines as the ACC increases for both networks (Fig. 5(e)). This trend indicates that a sparse network connectivity structure can enhance the working memory capacity of the improved SNAN model, which in turn improves the overall performance of the network. This finding aligns with complex network studies that suggest networks with low-coefficient connectivity are more efficient in facilitating signaling and information processing.[48–50] Moreover, the synaptic coupling of neuronal networks (g_{syn}) in SNAN and improved SNAN models escalates with increasing noise intensity (Fig. 5(f)). This suggests that a certain level of noise may act as a non-specific stimulus, enhancing the connection strength between neurons or the overall activity level. The g_{syn} of the SNN model was stable at 0.12 due to the absence of astrocytes, resulting in poor resistance to interference in the working memory task. In addition, compared to the other two models, the improved SNAN model exhibited moderate synaptic coupling strength, and the trend of coupling strength was flatter with the enhancement of noise intensity. This suggests that a moderate synaptic coupling strength can reach a balance between maintaining network stability and adapting to external disturbances, thus improving the information processing and retention efficiency of working memory.

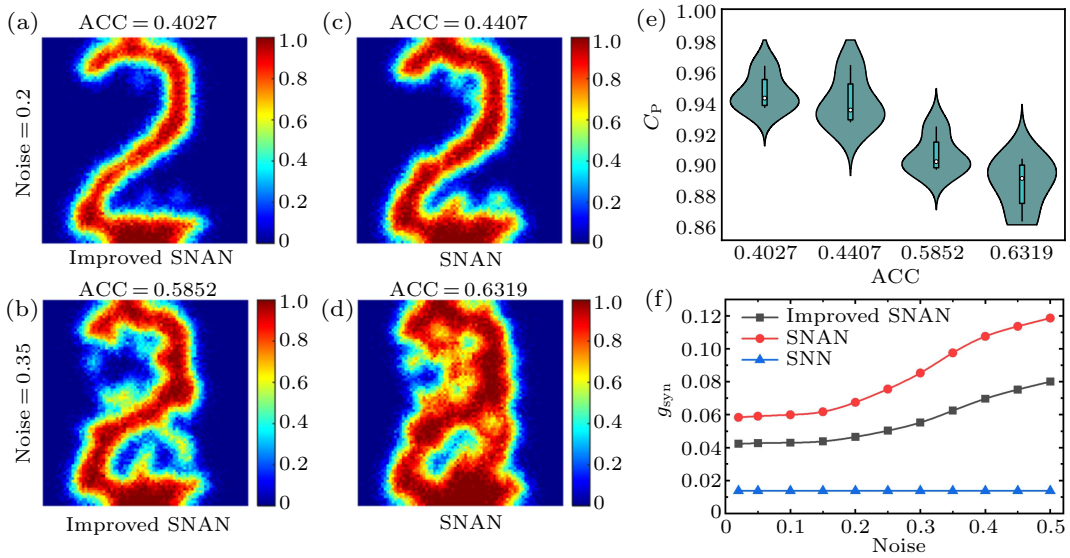


Fig. 5. Association between neuronal connection strength and working memory performance. (a)–(d) Heat maps showing the model's average neural connection strength at noise levels of 0.2 and 0.35. (e) Violin plots that illustrate the link between the SNAN model's working memory capacity (C_{P}) and ACC at various noise levels. (f) Impact of varying noise intensity on synaptic coupling (g_{syn}).

Benefiting from the modulation of 2-AG and glutamate, the improved SNAN model exhibits a moderate AFR and the neuronal firing duration is significantly prolonged. Compared to the SNAN model, the improved SNAN model shows a moderate AFR (Figs. 6(a) and 6(b)). In the improved SNAN model, 2-AG and glutamate jointly regulate the activity of astrocytes. This regulatory effect reduces the concentration requirement for PrSNs to release glutamate, thereby decreasing neuronal excitability compared to the SNAN model. The SNN model exhibited a lower AFR, with the maximum peak during the test phase not surpassing 45 Hz. Astrocytes enhance neuronal excitability by releasing gliotransmitters (e-SP action). In the SNN model, the absence of astrocytes leads to insufficient neuronal modulation, resulting in a low AFR. At a high noise intensity of 0.35, the AFR of the improved SNAN model exhibits a significant enhancement of approximately 50% (Fig. 6(c)). Astrocytes can enhance neuronal excitability and synaptic plasticity by strengthening e-SP action, thereby facilitating more efficient information processing within the network and enabling resistance to interference. This aligns with the conclusion that neurons employ nonlinear mechanisms, including high-gain amplification and positive feedback, to enhance information processing.[51–53]

Figure 6(d) shows the AFR for each model at a specific noise intensity throughout the experiment. The AFR changes in the neuronal layer are nearly synchronous with the input signals for image training and testing. This indicates that neurons can quickly respond transiently to external stimuli by gen-

erating a series of action potentials upon stimulus reception. The comparison reveals that the presence of astrocytes significantly improves the clarity and stability of the firing pattern. Taking the time point of 5.57 s as an example, it can be seen that in the SNN model without astrocytes, the neuron's firing activity was nearing its end and the firing pattern became blurred. However, when astrocytes are involved, they significantly lengthen the neuron's firing time and allow the firing pattern to remain clear, with the figures more sharply outlined and easily recognized. This is likely related to the role astrocytes play in signaling. Astrocytes influence the excitability of neurons by regulating the dynamics of calcium ions, which in turn has an effect on neuronal firing activity over a longer time scale.

In working memory tasks, astrocytes play a crucial role in the formation and maintenance of memory traces, which are closely related to fluctuations in Ca^{2+} concentration and can persist intracellularly for a long time. From the astrocyte layer slice images captured at specific time points ($t = 0.923$ s, 1.283 s, 1.599 s, 2.206 s), it can be observed that when new memory items are input, the existing memory traces in the astrocyte layer (represented as Ca^{2+} activity patterns) do not completely dissipate within a few seconds. Instead, the overlapping and coexistence of traces corresponding to different items (0, 1, 2, 3) are clearly visible (Figs. 7(e)–7(h)). This overlap indicates that astrocytes can integrate sequentially input information in working memory tasks, retaining a 'memory' of previous neural activity while processing current activity. Figures 7(i) and 7(j) illustrate the calcium signaling mechanism in neurons; the calcium signal exhibits a sustained propagation pattern with a significant time delay relative to glutamate signals, and its concentration peaks in the middle stage of training. Compared to the original SNAN model, the improved SNAN model shows a reduced Ca^{2+} concentration intensity, which highlights its enhanced network robustness — astrocytes can achieve optimal memory performance at lower Ca^{2+} concentrations.

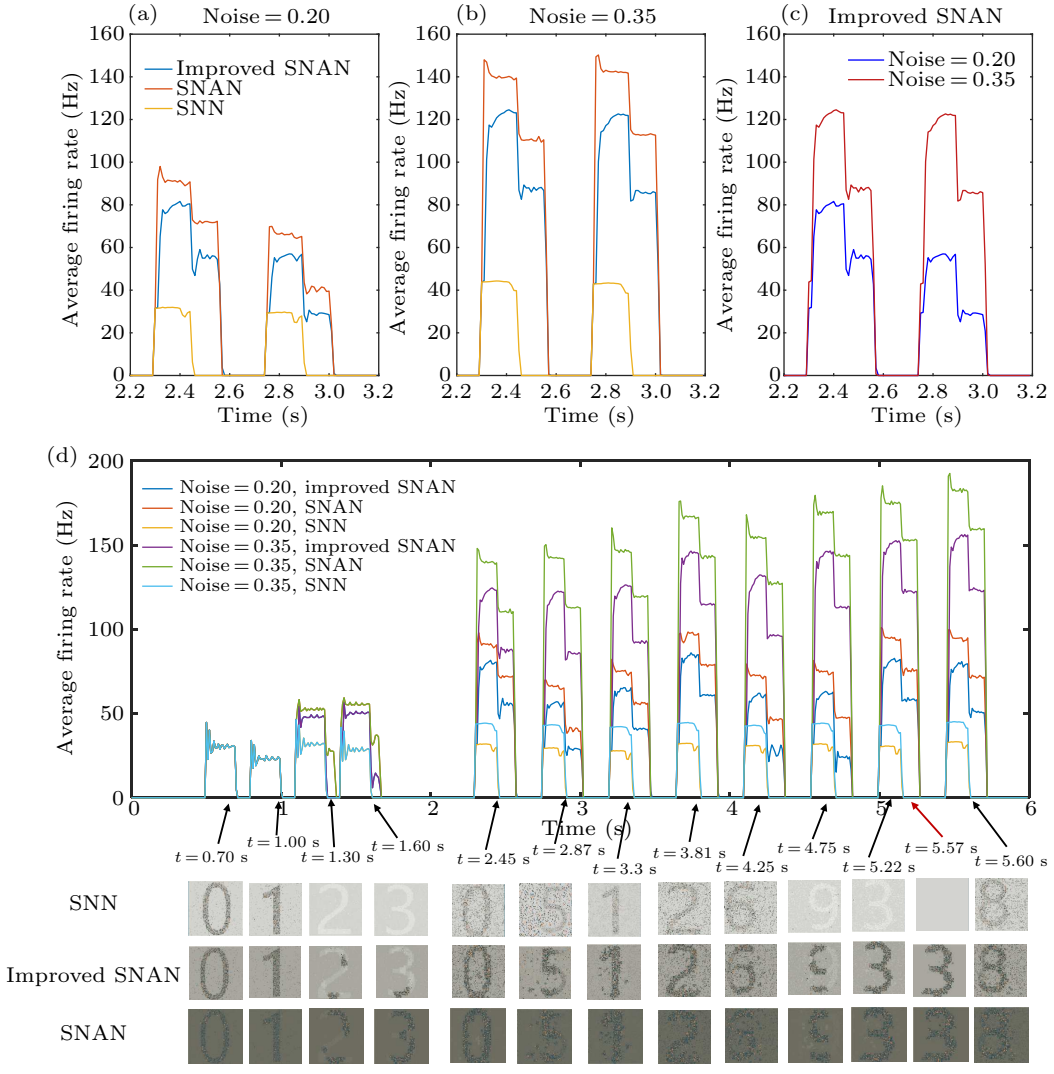


Fig. 6. Schematic representation of neuronal firing rate over time. (a) and (b) The average firing frequency for each model over 2.2 s to 3.2 s at 0.2 and 0.35 noise levels. (c) Average firing rate of the improved SNAN over 2.2 s to 2.3 s at 0.2 and 0.35 noise levels. (d) Average firing rate of the different models at 0.2 and 0.35 noise levels throughout the experiment.

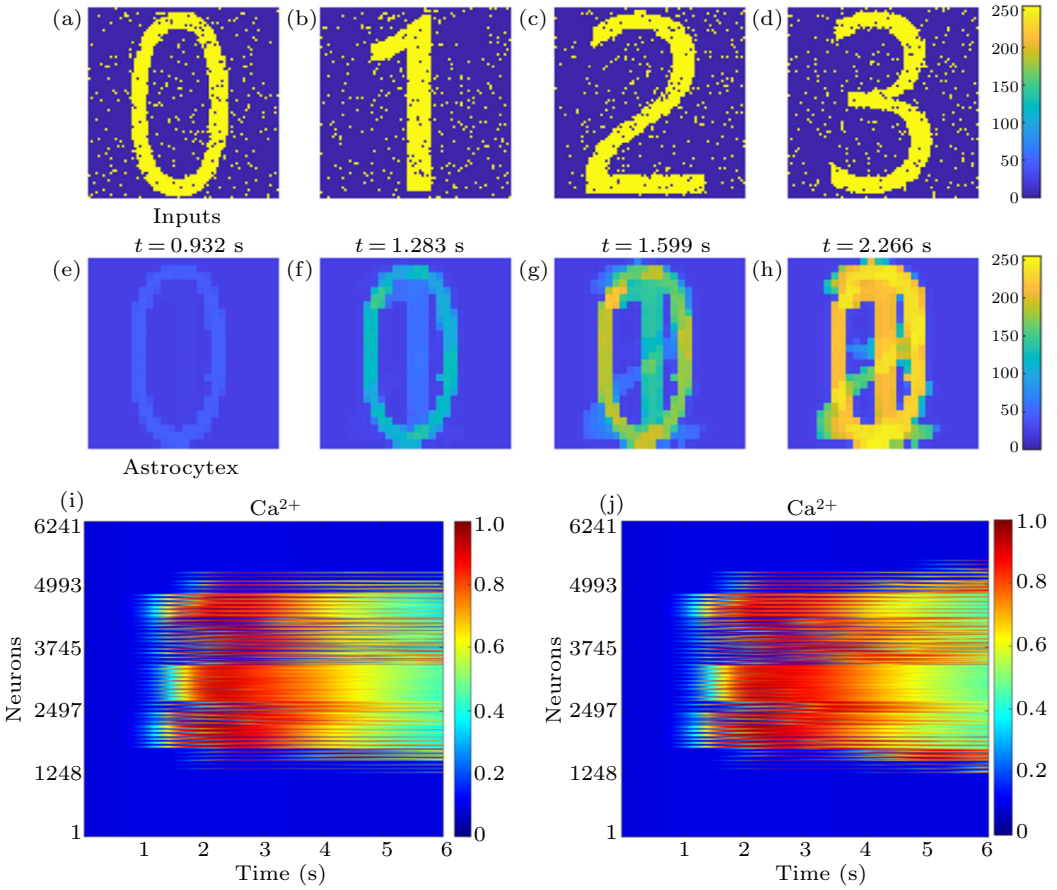


Fig. 7. Astrocyte responses during training, which demonstrate the mechanisms of neuronal calcium signal reception in neural networks. (a)–(h) Astrocyte response to various stimuli during training, showing distinct patterns. Changes in calcium ion concentration are represented by color gradients, ranging from blue to yellow, with green in between. (i)–(j) The schematic diagrams of neurons receiving calcium ion signals for both the improved SNAN and SNAN.

3.3. Generality of anti-interference performance in the improved SNAN

In addition, we compare the C_P of the improved SNAN model and the SNN model under different noise intensity and synaptic connection strength conditions, and further investigate the specific influence of the key model parameter — the maximum synaptic weight (w_{max}) — on working memory performance. The experiment consists of two groups: an SNN model and an improved SNAN model. In each group, we established three distinct w_{max} (0.02, 0.04, 0.06) to evaluate the impact of synaptic weights on C_P. It is demonstrated that in the absence of astrocytes, C_P increases with the increase in w_{max}. However, the improved SNAN model has a nonlinear feature. It is shown that under low noise intensity, an increase in w_{max} can slightly enhance C_P. Under high noise intensity, an increase in synaptic weights leads to a decrease in C_P, while smaller w_{max} can improve C_P.

The recalled images of the improved SNAN model and the model devoid of astrocytes are depicted at noise intensities of 0.15 and 0.30, as presented in Figs. 8(b) and 8(c). This shows that the improved SNAN model has better recall results at 0.30 noise intensity when w_{max} is lower, and there is no significant difference in recall values at 0.15 noise intensity. The recall results of the SNN without astrocytes, as depicted in Fig. 8(c), indicate that high w_{max} facilitates substantial recall of discharge results at a noise intensity of 0.15. However, the network demonstrates minimal memory recall at this same noise intensity. The results indicate that astrocytes participate in both memory formation and maintenance, and provide an anti-interference function in noisy environments.

We further analyzed the C_P of the SNAN and improved SNAN networks for numbers 0 to 7 as the noise intensity increased from 0.08 to 0.11 (Fig. 9(a)). The improved SNAN network exhibited peak working memory performance at a noise intensity of 0.1, which may be related to a resonance-like phenomenon, consistent with the discussion in Fig. 3(d). Except for input signal 1, the improved SNAN showed significant advantages in working memory. We speculate that the advantage of the improved SNAN will become more pronounced as the complexity of digit features increases. Figures 9(b)–9(e) depict the effects on working memory when SNAN and improved SNAN process more complex images. At a noise level of 0.10, the improved SNAN can reproduce the patterns of the input images more clearly and accurately, demonstrating its superior working memory performance. In contrast, the firing patterns of SNAN become irregular, and the clarity of the grid structure is impaired. Even when the noise level rises to 0.20, the improved SNAN still maintains clear firing patterns, and the grid structure remains clearly identifiable. This indicates

that the improved SNAN can retain and process information more effectively in the face of the complexity of image memory. Even under noise interference, the improved SNAN maintains a high degree of clarity in its firing patterns. The reason the improved SNAN performs better in memorizing complex images is that the refined astrocyte modulation mechanism enhances the neural network's ability to capture complex features and it has anti-interference capability against noise.

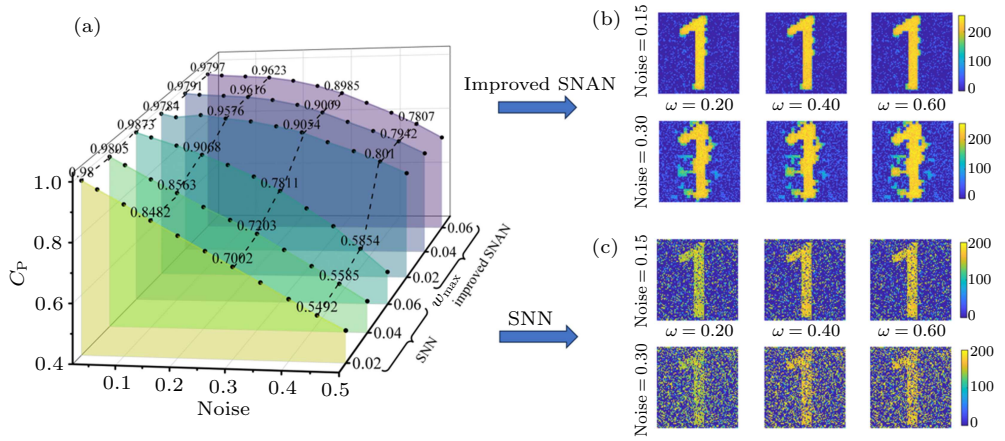


Fig. 8. Performance of the improved SNAN model and SNN model in WM tasks under varying noise and synaptic strength conditions. (a) Variation in performance metric (C_P) for working memory tasks at different noise levels, comparing the improved SNAN model to the SNN model. Color gradients in the graphs indicate variations in synaptic strength and model type. (b) Neuronal network's response to the digital '1' input in the improved SNAN model. Images illustrate the cue recall of the network across varying noise levels and synaptic strength (w) conditions. (c) Performance of SNN, similar to (b).

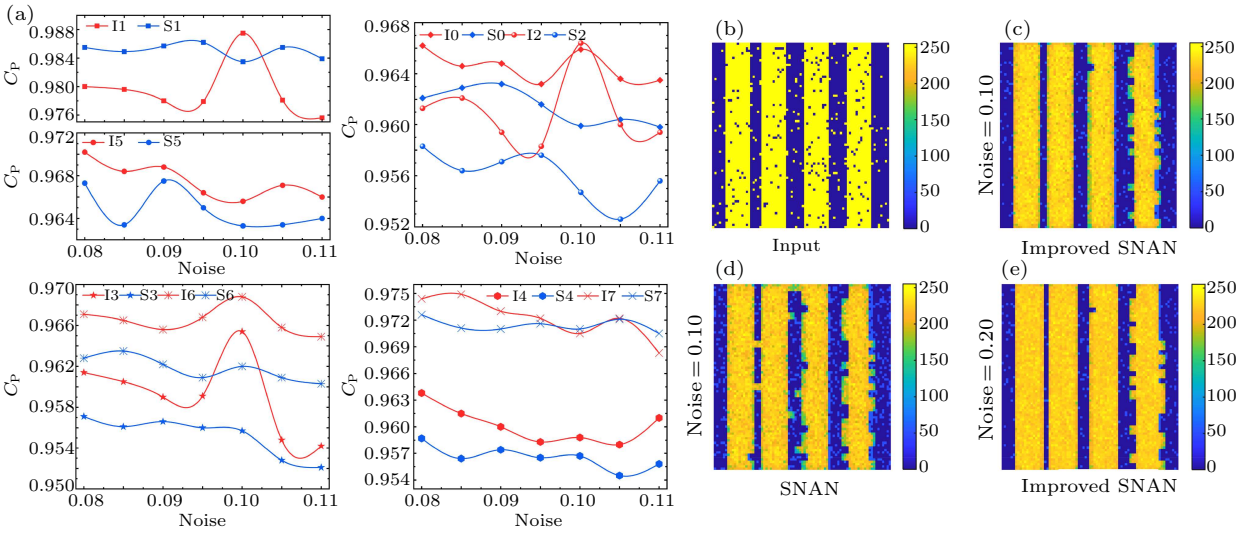


Fig. 9. (a) Working memory for individual digit signals in SNAN and improved SNAN networks across noise intensities. I0 to I7 represent the improved SNAN corresponding to numerical memory, while I0 to I7 represent the SNAN corresponding to numerical memory. (b)–(e) Working memory performance of SNAN versus improved SNAN for complex raster map input signals.

4. Conclusion

Working memory is a fundamental component of brain cognitive function, playing a crucial role in learning, the construction of long-term memory, and complex information processing. Its anti-interference ability and efficacy depend on the network structure and the balance of excitatory and inhibitory neurons within the nervous system. This study focused on the anti-interference ability of the spiking neuron–astrocyte network in working memory, providing new insights into understanding the neural mechanisms of working memory from a computational perspective.

Based on the Izhikevich neuron and astrocyte network, the 2-AG biological mechanism and the STDP rule are introduced, acting respectively on synaptic coupling strength (g_{syn}) and synaptic weights (w_{ij}) to regulate the coupling strength of the astrocyte network, thereby enhancing network heterogeneity. Through working memory tests, it was found that a scale-free network with 60% excitatory neurons achieved an optimal working memory performance of 0.9640, stressing the importance of network structure and neuron proportion. This formed the basis for the improved SNAN model, which realistically simulated brain synaptic connections.

The improved SNAN model proposed in this study performs superiorly in working memory tasks, especially in terms of its anti-interference performance. First, compared to the SNN model without astrocytes, both the SNAN model and the improved SNAN model demonstrated better performance, indicating that the presence of astrocytes is crucial for enhancing the working memory effect. Second, the improved

SNAN model with the 2-AG biological process outperformed the SNAN model, fully demonstrating that 2-AG plays an active role in promoting working memory and enhancing anti-interference ability. In a noisy environment, compared to SNN, the improved SNAN and SNAN models exhibited better anti-interference effects at moderate noise levels, but when the noise intensity was high, the working memory of both was significantly affected.

Furthermore, this study delved into the reasons the system with the 2-AG biological process could enhance anti-interference ability. The results suggested that it might be related to the secretion amount of glutamate and the network topology of the neuron–astrocyte system. Specifically, a lower average clustering coefficient of the network was associated with better working memory performance. In addition, there was an optimal value for the synaptic coupling strength, at which working memory performed optimally, and either too small or too large a synaptic coupling strength would adversely affect working memory performance.

In summary, through an in-depth study of the improved SNAN model, we analyzed the mechanism of the neuron-astrocyte network in working memory. It not only verified the positive effects of astrocytes and 2-AG on working memory and interference resistance but also revealed the relationships between factors such as the noisy environment, network topology, and synaptic coupling strength and working memory performance. These findings contribute to a greater understanding of the neural mechanisms of working memory and provide potential strategies and directions for enhancing cognitive function and addressing related cognitive impairment issues in the future. Future research could focus on synaptic plasticity, network sparsity, multi-item working memory modeling, network robustness, and self-repair mechanisms of astrocytes, continuously deepening the understanding of the neural basis of working memory through modeling.

Acknowledgements

This study was supported by the National Natural Science Foundation of China (Grant Nos. 12305054 and 12572032), the Guangdong Provincial Key Laboratory of Mathematical and Neural Dynamical Systems (Grant No. 2024B1212010004), and the Fundamental Research Funds for Central Universities, China University of Geosciences (Wuhan) (Grant No. CUGQT2023001).

References

[1] Alexander R, Aragón O R, Bookwala J, *et al*. 2021 *Neuroscience & Biobehavioral Reviews* **121** 220
[2] Miyake A, Friedman N P, Emerson M J, *et al*. 2000 *Cognitive Psychology* **41** 49
[3] Baddeley A D 2001 *American Psychologist* **56** 851
[4] Kolk S M, Rakic P 2022 *Neuropsychopharmacology* **47** 41
[5] Li H, Yan G, Luo W, *et al*. 2021 *Brain Structure and Function* **226** 1961
[6] Zhu J, Cheng Q, Chen Y, *et al*. 2020 *Neuron* **105** 934
[7] Spiegel I, Mardinly A R, Gabel H W, *et al*. 2014 *Cell* **157** 1216
[8] Zeltser L M, Seeley R J, Matthias H 2012 *Nature Neuroscience* **15** 1336
[9] Farhy-Tselnicker I, Allen N J 2018 *Neural Development* **13** 7
[10] Perea G, Navarrete M, Araque A 2009 *Trends in Neurosciences* **32** 421
[11] Scanziani M, Salin P A, Vogt K E, *et al*. 1997 *Nature* **385** 630
[12] Navarrete M, Araque A 2010 *Neuron* **68** 113
[13] Kang J, Jiang L I, Goldman S A, *et al*. 1998 *Nature Neuroscience* **1** 683
[14] Fiacco T A, Agulhon C, Taves S R, *et al*. 2007 *Neuron* **54** 611
[15] Binan L, Jiang A, Danquah S A, *et al*. 2025 *Cell* **188** 2141
[16] Simpson E H, Akam T, Patriarchi T, *et al*. 2024 *Neuron* **112** 718
[17] Saults J S, Cowan N 2007 *Journal of Experimental Psychology: General* **136** 663
[18] Jiang S, Song Y, Kang H, *et al*. 2021 *ACS Applied Materials & Interfaces* **14** 3385
[19] Guerrieri A, Lattanzio V, Palmisano F, *et al*. 2006 *Biosensors & Bioelectronics* **21** 1710
[20] Song Y, Guo L, Man M, *et al*. 2024 *Pattern Recognition* **155** 110672
[21] Iglesias J, Eriksson J, Grize F, *et al*. 2005 *Biosystems* **79** 11
[22] Eshraghian J K, Ward M, Neftci E O, *et al*. 2023 *Proceedings of the IEEE* **111** 1016
[23] Wang J, Zhao D, Du C, *et al*. 2024 *iScience* **28** 112660
[24] Gordleeva S, Tsybina Y, Krivonosov M, *et al*. 2023 *IEEE Transactions on Neural Networks and Learning Systems* **36** 881
[25] Zhuoheng G, Liqing W, Xin Z, *et al*. 2024 *Cognitive Neurodynamics* **18** 503
[26] Naghieh P, Delavar A, Amiri M, *et al*. 2023 *iScience* **26** 108241
[27] Palaba T, Ylmaz E 2025 *Nonlinear Dynamics* **113** 8991
[28] Lu L, Gao Z, Wei Z, *et al*. 2023 *Chaos* **33** 013127
[29] Keith J M, Apodaca R, Xiao W, *et al*. 2008 *Bioorganic & medicinal chemistry letters* **18** 4838
[30] Mahmoud S, Gharagozloo M, Simard C, *et al*. 2019 *Cells* **8** 184
[31] Gordleeva S, Tsybina Y, Krivonosov M, *et al*. 2021 *Frontiers in Cellular Neuroscience* **15** 631485
[32] Santello M, Volterra A 2009 *Neuroscience* **158** 253
[33] Rodríguez-Arellano J J, Parpura V, Zorec R, *et al*. 2016 *Neuroscience* **323** 170
[34] Izhikevich E M 2003 *IEEE Transactions on Neural Networks* **14** 1569
[35] Liu C, Wang J, Yu H, *et al*. 2015 *Communications in Nonlinear Science and Numerical Simulation* **28** 10
[36] Lu L, Yi M and Liu L 2022 *Science China Technological Sciences* **65** 1661
[37] Kampakis S 2012 *Soft Computing* **16** 943
[38] Kanakov O, Gordleeva S, Ermolaeva A, *et al*. 2019 *Phys. Rev. E* **99** 012418
[39] Esir P M, Gordleeva S Y, Simonov A Y, *et al*. 2018 *Phys. Rev. E* **98** 052401
[40] Caporale N and Dan Y 2008 *Annual Review of Neuroscience* **31** 25
[41] Feldman D E 2012 *Neuron* **75** 556
[42] Pfister J P, Gerstner W 2006 *The Journal of neuroscience* **26** 9673
[43] Ullah G, Jung P, Cornell-Bell A H 2006 *Cell Calcium* **39** 197
[44] Kazantsev V B, Asatryan S Y 2011 *Phys. Rev. E* **84** 031913
[45] Aghazadeh R, Salimi-Nezhad N, Arezoomand F, *et al*. 2025 *Neural Networks* **182** 106934
[46] Zhou T, Yan G, Wang B H 2005 *Phys. Rev. E* **71** 046141
[47] Tsybina Y, Kastalskiy I, Krivonosov M, *et al*. 2022 *Neural Computing and Applications* **34** 9147
[48] Ghavasieh A, De Domenico M 2024 *Nature Physics* **20** 512
[49] Hens C, Harush U, Haber S, *et al*. 2019 *Nature Physics* **15** 403
[50] Zachariah M K, Coleman G T, Mahns D A, *et al*. 2001 *Journal of Neurophysiology* **86** 900
[51] Amiri M, Hosseinmardi N, Bahrami F, *et al*. 2013 *Journal of Computational Neuroscience* **34** 489
[52] Squadrani L, Wert-Carvajal C, Müller-Komorowska D, *et al*. 2024 *Communications biology* **7** 852
[53] Yamamoto M and Takano T 2025 *Cells* **14** 1936
[54] Lv G, Xu T, Chen F, *et al*. 2024 *Chin. Phys. B* **33** 028704
[55] Li Z J, Zhang J 2024 *Chin. Phys. B* **33** 128701
[56] Oberheim N A, Wang X, Goldman S, *et al*. 2006 *Trends in Neurosciences* **29** 547
[57] Oberheim N A, Takano T, Han X, *et al*. 2009 *Journal of Neuroscience* **29** 3276
[58] Halassa M M, Fellin T, Takano H, *et al*. 2007 *Journal of Neuroscience* **27** 6473